SANDIA REPORT

SAND2016-9319
Unlimited Release
Printed Month and Year

Measurements and Modeling of Black-Carbon Aerosols in the Arctic

Ray P. Bambha, Brian W. LaFranchi, Paul E. Schrader, Daniel A. Lucero, Mark D. Ivey, Hope A. Michelsen

Prepared by
Sandia National Laboratories
Albuquerque, New Mexico 87185 and Livermore, California 94550

Sandia National Laboratories is a multi-mission laboratory managed and operated by Sandia Corporation, a wholly owned subsidiary of Lockheed Martin Corporation, for the U.S. Department of Energy's National Nuclear Security Administration under contract DE-AC04-94AL85000.

Issued by Sandia National Laboratories, operated for the United States Department of Energy by Sandia Corporation.

Available to DOE and DOE contractors from
U.S. Department of Energy
Office of Scientific and Technical Information
P.O. Box 62
Oak Ridge, TN 37831

Telephone: (865) 576-8401
Facsimile: (865) 576-5728
E-Mail: reports@osti.gov
Online ordering: http://www.osti.gov/scitech

Available to the public from
U.S. Department of Commerce
National Technical Information Service
5301 Shawnee Rd
Alexandria, VA 22312

Telephone: (800) 553-6847
Facsimile: (703) 605-6900
E-Mail: orders@ntis.gov
Online order: http://www.ntis.gov/search

SAND2016-9319
Unlimited Release
Printed Month Year

Measurements and Modeling of Black-Carbon Aerosols in the Arctic

Ray P. Bambha,[1] Brian W. LaFranchi,[2] Paul E. Schrader,[2] Daniel A. Lucero,[3] Mark D. Ivey,[3]
Hope A. Michelsen[2]
[1]Remote Sensing Department
[2]Combustion Chemistry and Diagnostics Department
Sandia National Laboratories
P. O. Box 969
Livermore, California 94551
[3]Atmospheric Sciences Department
P.O. Box 5800
Albuquerque, New Mexico 87185

Abstract

We have made the first continuous measurements of black carbon in Barrow, Alaska at the ARM aerosol-observing site at the NOAA Barrow Observatory using a Single-Particle Soot Photometer (SP2). These data demonstrate that BC particles are extremely small, and a majority of the particles (by number density) are smaller than 0.5 fg, the lower limit of reliability of the SP2.

We developed the first numerical model capable of quantitatively reproducing the laser-induced incandescence (LII) and scattering signals produced by the SP2, the industry-standard BC instrument. Our model reproduces the SP2 signal temporally and spectrally and demonstrates that the current SP2 optical design allows substantial contamination of LII on the scattering signal.

We ran CAM5-SE in nudged mode, i.e., by constraining the transport used in the model with meteorological data. The results demonstrate the problem observed previously of under-predicting BC at high latitudes. The cause of the discrepancy is currently unknown, but we suspect that it is associated with scavenging and rainout mechanisms.

ACKNOWLEDGMENTS

We thank Anne Jefferson, Ross Burgener, and Bryan Thomas for graciously allowing us to deploy our instrument in the NOAA BRW Station and attach our instrument to their inlet system. We thank Walter Brower, Jimmy Ivanoff, and Josh Ivanoff for helping us navigate our way to deployment in Barrow. We thank Gavin McMeeking (DMT) for sharing information about the SP2 instrument that enabled us to predict its temporal response, Daniel Strong (Sandia) for creating the rendition of the experimental setup shown in Fig. 1, Amy Halloran for helpful suggestions, Chris Sorensen for pointing out that R_g should increase with temperature, and Beth Rieken for assistance with data processing. This work was funded by the Laboratory Directed Research and Development program at Sandia National Laboratories. The thermodenuder, CPMA, and LII-model development were funded by the Division of Chemical Sciences, Geosciences, and Biosciences, the Office of Basic Energy Sciences, the US Department of Energy. Sandia National Laboratories is a multi-mission laboratory managed and operated by Sandia Corporation, a wholly owned subsidiary of Lockheed Martin Corporation, for the U.S. Department of Energy's National Nuclear Security Administration under contract DE-AC04-94AL85000.

CONTENTS

1. Introduction **8**
1.1 Black-Carbon Instrumentation **8**
1.2 Arctic Field Measurements of Black Carbon **9**
1.3 Atmospheric Modeling of Black Carbon **10**

2. Black-Carbon Instrumentation **11**

3. Arctic Field Measurements of Black Carbon **15**

4. Atmospheric Modeling of Black Carbon **19**

5. Conclusions **21**

FIGURES

Figure 1. Experimental setup for CW-LII-signal collection 11
Figure 2. Modeled and measured temporal profiles of CW LII and scattering signal 12
Figure 3. SP2 installed at the NOAA BRW Station. 15
Figure 4. Photograph of the NOAA BRW Station. 15
Figure 5. Time series of total black carbon mass measured by SP2 at the NOAA BRW Station. 16

NOMENCLATURE

AAOD	Aerosol absorption optical depth
ARCPAC	Aerosol, Radiation, and Cloud Processes affecting Arctic Climate
ARCTAS	Arctic Research of the Composition of the Troposphere from Aircraft and Satellite
AERONET	AErosol RObotic NETwork
BC	Black carbon
CPMA	Centrifugal particle mass analyzer
CW	Continuous wave
DMA	Differential mobility analyzer
DOE	Department of Energy
FINN	Fire INventory from NCAR
HIPPO	HIAPER Pole-to-Pole Observations
LII	Laser-induced incandescence
NCAR	National Center for Atmospheric Research
NOAA	National Oceanic and Atmospheric Administration
NSF	National Science Foundation
PSAP	Particle Soot Absorption Photometer
SNL	Sandia National Laboratories
SP2	Single-Particle Soot Photometer

1. INTRODUCTION

Growing evidence suggests that black carbon (BC) particles contribute significantly to global climate change and are largely responsible for the enhanced warming of the Arctic (~twice that of the global rate) [1, 2]. Because of the relatively short atmospheric lifetimes of particulates compared to CO_2 and the large radiative forcing of BC aerosols (23-65% that of CO_2), BC reductions are being considered as a viable near-term climate-change mitigation approach [3]. Assessing the effectiveness of such a strategy, however, will require better estimates of BC climate forcing, which are hampered by large uncertainties associated with a paucity of atmospheric observational constraints, particularly in the Arctic, and poorly represented BC physical and optical properties in climate models [4, 5]. In order to reduce the uncertainties of Arctic climate forcing of BC by combining Arctic field observations, laboratory experiments, and modeling, we (1) combined laboratory experiments and modeling to characterize state-of-the-art commercial BC instrumentation and (2) deployed instrumentation to characterize the abundance of BC-containing aerosols in the Arctic.

Aerosol models tend to overestimate BC concentrations at all altitudes and latitudes [4-9]. Model-measurement discrepancies are often less severe at the Earth's surface, however, and models may even underestimate BC surface concentrations under some conditions, particularly in the Arctic [4, 5, 10, 11]. Discrepancies between models and Arctic measurements appear to vary with season [12-14]; underestimations of surface BC loading are largest for the spring, and models often fail to capture the increase in BC loading leading to Arctic haze [4, 13, 14]. These discrepancies have been attributed to misrepresentation of wet deposition rates [11, 13] and coarse model resolution [15]. There are, however, very few data sets available for the Arctic. Comparisons between models and measurements for Arctic BC loading are based on data from a couple of aircraft campaigns for the SP2 [4, 5, 7, 11-13], filter-based data from the Particle Soot Absorption Photometer (PSAP) recorded at the NOAA BRW Station [12-14], and ground-based remote sensing observations from the AErosol RObotic NETwork (AERONET) [4, 5].

ARCTAS Arctic Research of the Composition of the Troposphere from Aircraft and Satellite [16]

ARCPAC Aerosol, Radiation, and Cloud Processes affecting Arctic Climate [17]

HIPPO HIAPER Pole-to-Pole Observations [18]

PSAP Particle Soot Absorption Photometer [19]

AERONET AErosol RObotic NETwork [20]

1.1. Black-Carbon Instrumentation

Mature soot absorbs strongly and broadly across optical wavelength regions and is refractory with a sublimation temperature of ~4000 K. Clean, mature soot is composed of small "primary" particles of polycrystalline graphite 10-50 nm in diameter covalently bound into dendritic aggregates of varying size with branched-chain structures typically characterized by fractal dimensions of 1.7-1.9 [21-25]. When these particles age in the atmosphere and become coated

with semi-volatile coatings, the morphology of these particles can collapse, resulting in and increase in the fractal dimension and changes to particle surface areas and optical properties. Many studies have demonstrated such effects when particles are coated with oxygenated hydrocarbons [26-36] or sulphuric acid [31, 37-40]. For some coatings (e.g., heptane, oleic acid, glutaric acid, sulphuric acid, and dioctyl sebacate) this restructuring is irreversible, such that the particles retain a compressed morphology when the coatings are removed in a thermodenuder [27, 30, 31, 35, 39, 40]. For succinic acid coatings, however, the restructuring appears to be insignificant [30].

Laser-induced incandescence (LII) is a diagnostic technique that has been used extensively to measure soot-particle abundances and physical properties under a wide range of conditions, e.g., in engines [41-47], flames [48-54], exhaust streams [37, 55-57], and the ambient atmosphere [58-64]. The implementation of LII involves heating soot particles in an intense laser field to temperatures as high as 4000 K and measuring the resulting incandescence from the hot particles [65]. The signal magnitude is related to the particle volume fraction or mass. It is also nonlinearly dependent on the particle temperature. While laser absorption is responsible for heating the particle, conductive cooling is the dominant cooling mechanism under non-vacuum conditions when sublimation can be ignored. The balance of heating and cooling mechanisms determines particle temperature, which controls LII signal as a function of time. When a nanosecond pulsed laser system is used to heat the particles, as is typical for combustion studies, conductive cooling can be ignored on the timescale of absorptive heating, and the LII peak temperature is directly related to the laser fluence and particle absorption cross section. When a CW laser is used, as is common for atmospheric-soot measurements, the laser-particle interaction time is on the order of microseconds, and conductive cooling competes with absorptive heating.

Particle aggregation effects, such as aggregate size and morphology, influence the average particle-surface area available to interact directly with the bath gas. Shielding of some primary particles within an aggregate by other primary particles is predicted to cause large aggregates to have lower effective surface areas per primary particle than smaller aggregates [66-74]. Experiments by Kuhlmann et al. [69] to confirm these effects demonstrated only small changes to the decay rate with increasing aggregate size. Experimental confirmation of these effects performed by Bladh et al. [71], in contrast, demonstrated more significant changes to the decay rate than anticipated or explained by aggregate size. Bladh et al. [71] suggested that additional effects could be related to aggregate morphology. Bambha et al. [75] experimentally demonstrated significant reductions in LII signal-decay rates with an increase in fractal dimension. The behavior can be explained by lower conductive-cooling rates caused by an increase in primary-particle shielding and a decrease in effective-surface area for the restructured (i.e., collapsed) particle.

The effect of particle morphology on scattering cross sections is less obvious. Some theories predict that the scattering cross section should decrease with increasing fractal dimension because either (1) the aggregate size is reduced or (2) multiply scattered waves at the aggregate core destructively interfere [25, 37, 76, 77]. Other studies predict that the increased scattering interactions between primary particles should lead to an increase in the scattering cross section with increasing fractal dimension [78, 79].

We have studied and characterized the effects of BC particle morphology on measurements made using a commercial instrument known as the Single-Particle Soot Photometer (SP2) [60]. This instrument has become a common instrument for measuring atmospheric BC, but it has not been well characterized under a range of relevant conditions. The SP2 employs a continuous-wave laser induced incandescence (LII) technique that is poorly understood with respect to systematic biases, and its sensitivity to small BC particles (<~140 nm mobility diameter) is poor. Nonetheless, the SP2 has been deployed at numerous lower latitude sites and on aircraft missions.

1.2. Arctic Field Measurements of Black Carbon

A recent DOE workshop on the leading uncertainties in climate models concluded that there are significant uncertainties in the physics and chemistry of aerosols and aerosol-cloud interactions, leading to systematic errors in climate-model representations of aerosol and cloud radiative effects. General circulation models have particular problems simulating aerosols in the upper troposphere (where they overestimate aerosol concentrations) and at high latitude (where they underestimate concentrations). These problems stem, in part, from a paucity of observations of aerosol global distributions and properties, such as composition, mixing, morphology, and size distribution. In particular, there is a severe lack of information on aerosol vertical distributions and a need for field studies to provide information about aerosol, cloud features, and their relationships to guide model parameterizations and validation. Atmospheric measurements of BC are especially scarce, in part because state-of-the-art instrumentation is not easily fieldable for remote, continuous operation.

We deployed an SP2 in Barrow, Alaska at the ARM aerosol-observing site at the National Oceanic and Atmospheric Administration (NOAA) Barrow Observatory, i.e., the NOAA BRW Station. Although BC is measured using filter-based instrumentation in Barrow, our measurements are the first continuous measurements of BC in Barrow using an SP2.

[Blank page following section.]

2. BLACK-CARBON INSTRUMENTATION

We have developed a model for LII that reproduces and predicts the temporal response of the LII signal over a wide range of laser fluences [65, 80-82]. For pulsed-laser applications, this model solves the energy- and mass-balance equations during and after the laser pulse and includes heating by laser absorption, surface oxidation, and annealing, cooling by conduction to the surrounding atmosphere, sublimation, radiative emission, and thermionic emission, and mass loss by sublimation, non-equilibrium desorption, and oxidation. The particles are allowed to anneal, which influences conductive cooling rates and absorptive heating rates. The model has been validated with data taken in flames using 532 and 1064 nm laser heating over two orders of magnitude in laser fluence. It reproduces measured LII signal and particle-temperature temporal profiles. We have recently adapted it for characterizing the behavior of an atmospheric black-carbon instrument that produces LII signal from single particles injected intracavity into a CW-laser beam with time-resolved broadband LII-signal detection (shown in Fig. 1). Using this model, we have shown that factors that influence conductive-cooling rates, such as primary-particle size and aggregate size and morphology, have a strong influence on whether particles reach the sublimation point and whether the technique is linear with particle mass [83].

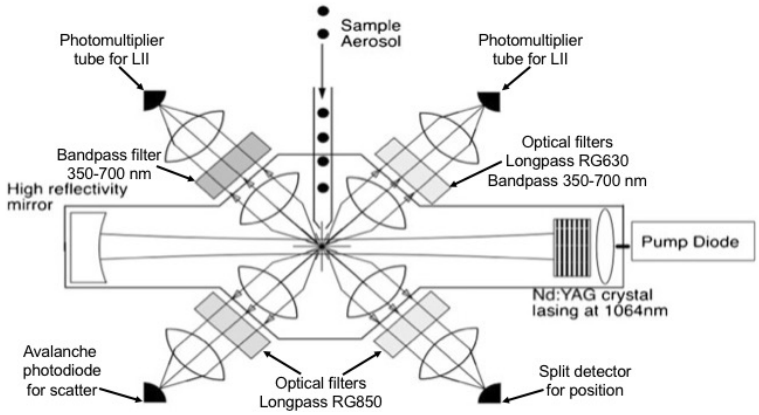

Figure 1. Experimental setup for CW-LII-signal collection. Particles are delivered to the Single-Particle Soot Photometer (SP2, Droplet Measurement Technologies) at atmospheric pressure. A nozzle, perpendicular to the laser beam and detection axis, directs the aerosol to the center of the laser cavity where the beam waist is ~1.1 mm. Particles drift through the laser beam and are detected one at a time by two PMTs equipped with different broadband filters for two-color LII and an avalanche photodiode for elastic scatter. Adapted from Schwarz *et al.* [60].

The intracavity-beam intensity of this instrument is on the order of 10^6 W/cm^2, and the particles traverse the beam on timescales on the order of 10 μs before they exit the beam or are vaporized. The laser-particle interaction is determined by the drift time of the particle through the laser beam [84] and is comparable to particles interacting with a high-fluence laser pulse (~3 J/cm^2) with a pulse duration of ~10 μs [83]. Ideally, under normal operating conditions, the particles are heated to the sublimation temperature, and the maximum of the LII signal occurs at the sublimation temperature and is linearly dependent on the particle mass.

The temporal distributions measured using CW LII are sensitive to particle-aggregate morphology and size and may also be useful for inferring aggregate morphologies or exposed

particle-surface areas [83]. Figure 2a shows LII temporal profiles for three aggregate sizes and two aggregate morphologies measured using an SP2. Because the SP2 measures LII temporal profiles of individual particles, the data can be binned by particle size within a distribution based on LII signal intensity. Figure 2a shows that LII signal occurs earlier (relative to the time the particle enters the laser beam) for more compact particles (D_f=2.4) than for less compact particles (D_f=1.9). The differences are related to the increased surface area available for conductive cooling for the less compact particles and more effective competition between conductive cooling and absorptive heating as the particles transit the laser beam. This technique, combined with the model, might be capable of providing information about particle exposed-surface area or morphology but will require more refinement for the quantitative assessment of such parameters. In addition, this technique will only provide information about the aggregate morphology or surface area as long as the particles are not coated with a volatile coating, which can similarly influence the signal timing.

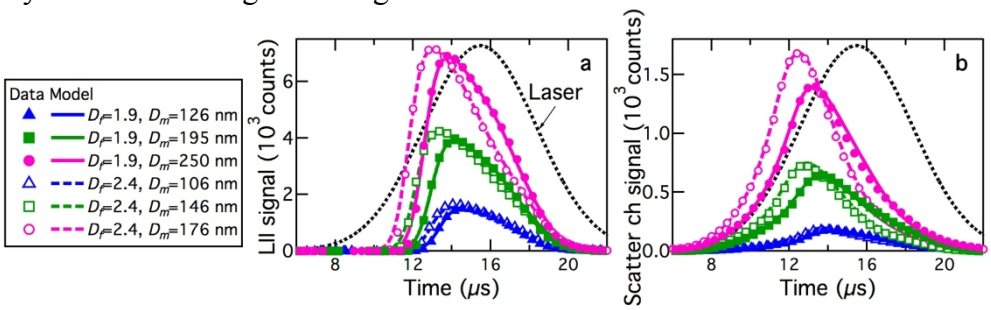

Figure 2. Modeled and measured temporal profiles of CW LII and scattering signal. Profiles are shown for (a) CW LII and (b) scattering signal for aggregates with selected sizes and morphologies. Symbols represent average temporal profiles from 50 particles for each size/morphology. Profiles were recorded for particles with average fractal dimensions of 1.9 and 2.4, as indicated in the legend. Lines indicate results from an LII model. This figure is adapted from Bambha and Michelsen [83].

Figure 2b shows the corresponding predicted scattering signal measured simultaneously with the LII signal. These results confirm the timing of the signal and provide information about the particle optical properties. Results from the scattering calculations suggest that the radius of gyration of the aggregates increases rapidly when the particle temperature hits the sublimation point, i.e., the aggregates pop like popcorn during sublimation [83].

Using the results of this work, we procured a new SP2 with filters, detectors, and amplifiers built to our specification, and we are performing side-by-side comparisons with the standard SP2, which will generate critical feedback to the vendor and community.

[Blank page following section.]

3. ARCTIC FIELD MEASUREMENTS OF BLACK CARBON

We deployed an SP2 at the National Oceanic and Atmospheric Administration (NOAA) Barrow Observatory, i.e., the NOAA BRW Station, which is part of the ARM aerosol-observing site in Barrow, Alaska. This instrument is part of the Arctic Methane, Carbon Aerosols, and Tracers Study (AMCATS) and is co-located with, and on the same inlet as, the other aerosol instruments at the NOAA BRW Station. We have been making measurements of BC in Barrow since February 2016. Photographss of the instrument and co-located instruments are shown in Fig. 3, and a photograph of the NOAA BRW Station and inlet are shown in Fig. 4.

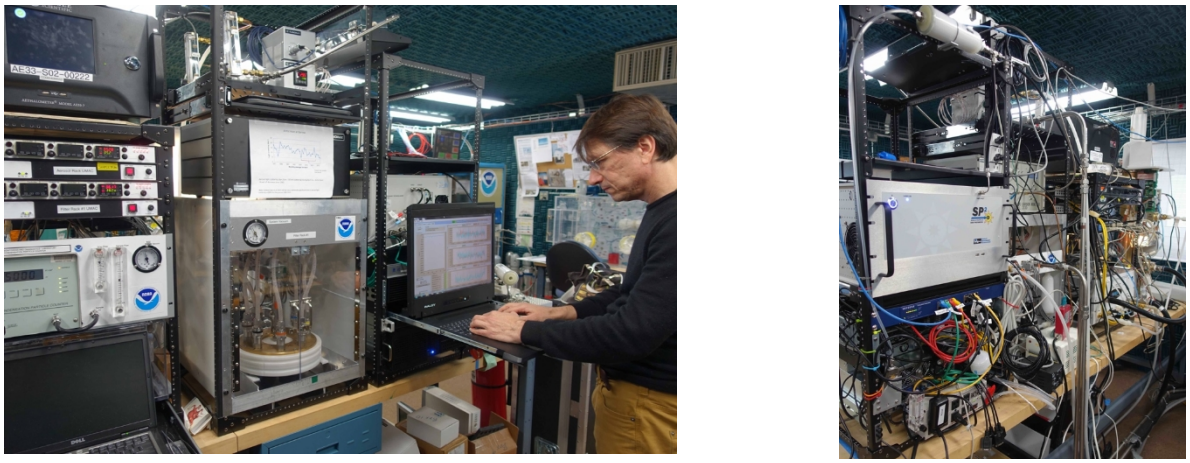

Figure 3. SP2 installed at the NOAA BRW Station. The SP2 is on the same inlet as several other instruments in the aerosol suite. The SP2 rack includes a computer for external communication, a data storage unit, a keyboard-video-mouse unit, and an uninterruptible power supply.

Figure 4. Photograph of the NOAA BRW Station. The tall stack protruding from the shelter is the aerosol inlet.

The instrument was calibrated using a suspension of fullerene agglomerates in water, aspirated through a nebulizer into a diffusion dryer and differential mobility analyzer (DMA). Voltages on the DMA were set to select mobility diameters of selected sizes, the masses for which had been calibrated using a centrifugal particle mass analyzer (CPMA) at Sandia. SP2 histograms were

recorded for each size distribution, and the maxima of the modes in the SP2 histograms were matched to the peaks of the modes of the masses given by the CPMA. Once fully installed and running in Barrow, the SP2 required maintenance, cleaning, and calibration at an interval of approximately every 3 months.

The calibrated Arctic data demonstrate that BC mass is highly variable as a function of time during the winter and early spring in Barrow, as shown in Fig. 5. These high-resolution BC measurements will allow detailed comparisons to be made for the first time between high-resolution atmospheric transport models and measurements over multiple months and seasons. These comparisons will provide a unique opportunity to refine models of the atmospheric processing of black carbon.

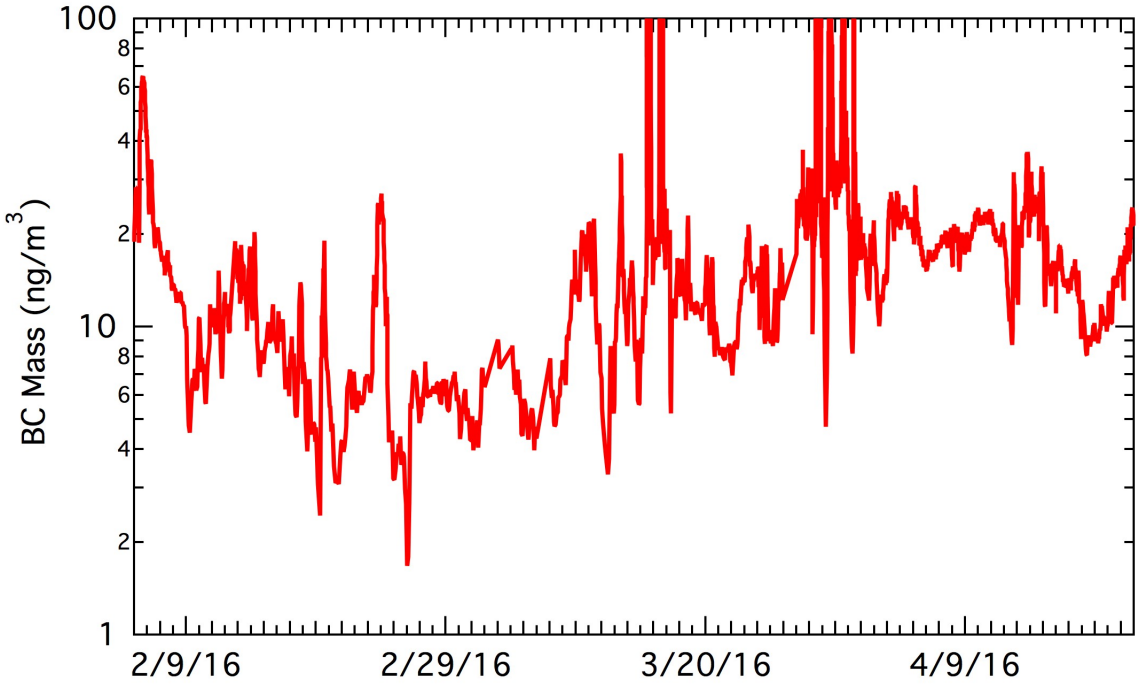

Figure 5. Time series of total black carbon mass measured by SP2 at the NOAA BRW Station.

[Blank page following section.]

5. CONCLUSIONS

We have performed experiments to characterize state-of-the-art instrumentation for black carbon measurements in the atmosphere. We have deployed this instrumentation in the Arctic, making continuous measurements of black carbon in Barrow, Alaska. The results show considerable variability in black-carbon concentration over the winter and spring.

[Blank page following section.]

6. REFERENCES

[1] IPCC. Climate Change 2007: The Physical Science Basis. Contribution of Working Group I to the Fourth Assessment Report of the Intergovernmental Panel on Climate Change. Solomon S, Qin D, Manning M, Chen Z, Marquis M, Averyt K, et al., editors. Cambridge, UK and New York, NY: Cambridge University Press; 2007.

[2] Quinn PK, Stohl A, Arneth A, Bernsten T, Burkhart JF, Christensen J, et al. AMAP Technical Report No. 4: The impact of black carbon on Arctic climate. Oslo, Norway2011.

[3] Shindell D, Kuylenstierna JCI, Vignati E, van Dingenen R, Amann M, Klimont Z, et al. Simultaneously mitigating near-term climate change and improving human health and food security. Science 2012;335:183-9.

[4] Koch D, Schulz M, Kinne S, McNaughton C, Spackman JR, Balkanski Y, et al. Evaluation of black carbon estimations in global aeorosl models. Atmos Chem Phys 2009;9:9001-26.

[5] Koch D, Schulz M, Kinne S, McNaughton C, Spackman JR, Balkanski Y, et al. Corrigendum to "Evaluation of black carbon estimations in global aeorosl models" published in Atmos. Chem. Phys., 9, 9001-9026, 2009. Atmos Chem Phys 2010;10:79-81.

[6] Reference on gasoline engine particulates.

[7] Fan S-M, Schwartz JP, Liu J, Fahey DW, Ginoux P, Horowitz LW, et al. Inferring ice formation processes from global-scale black carbon profiles observed in the remote atmosphere and model simulations. J Geophys Res 2012;117:D23205.

[8] Bond TC, Doherty SJ, Fahey DW, Forster PM, Berntsen T, DeAngelo BJ, et al. Bounding the role of black carbon in the climate system: A scientific assessment. J Geophys Res Atmos 2013;118(11):5380-552.

[9] Reddington CL, McMeeking GR, Mann GW, Coe H, Frontoso MG, Liu D, et al. The mass and number size distribution of black carbon aerosol over Europe. Atmos Chem Phys 2013;13:4917-39.

[10] Ma P-L, Rasch PJ, Fast JD, Easter RC, Gustafson WI, Jr., Liu X, et al. Assessing the CAM5 physics suite in the WRF-Chem model: Implementation evaluation, and resolution sensitivity. Geoscientific Model Development Discussions 2013;6:6157-218.

[11] Liu X, Easter RC, Ghan SJ, Zaveri RA, Rasch PJ, Shi X, et al. Toward a minimal representation of aerosols in climate models: Description and evaluation in the Community Atmosphere Model CAM5. Geoscientific Model Development 2012;5:709-39.

[12] Breider TJ, Mickley LJ, Jacob DJ, Wang Q, Fisher JA, Chang RY-W, et al. Annual distributions and sources of Arctic aerosol components, aerosol optical depth, and aerosol absorption. J Geophys Res Atmos 2014;119:4107-1424.

[13] Wang Q, Jacob DJ, Fisher JA, Mao J, Leibensperger EM, Carouge CC, et al. Sources of carbonaceous aerosols and deposited black carbon in the Arctic in winter-spring: Implications for radiative forcing. Atmos Chem Phys 2011;11:12453-73.

[14] Lee YH, Lamarque J-F, Flanner MG, Jiao C, Shindell DT, Bernsten T, et al. Evaluation of preindustrial to present-day black carbon and its albedo forcing from Atmospheric Chemistry and Climate Model Intercomparison Project (ACCMIP). Atmos Chem Phys 2013;13:2607-34.

[15] Ma P-L, Rasch PJ, Fast JD, Easter RC, Gustafson WI, Jr., Liu X, et al. Assessing the CAM5 physics suite in the WRF-Chem model: Implementation, resolution sensitivity, and a first evaluation for a regional case study. Geoscientific Model Development Discussions 2014;7:755-78.

[16] Jacob DJ, Crawford JH, Maring H, Clarke AD, Dibb JE, Emmons LK, et al. The Arctic Research of the Composition of the Troposphere from Aircraft and Satellites (ARCTAS) mission: Design, execution, and first results. Atmos Chem Phys 2010;10:5191-212.

[17] Brock CA, Cozic J, Bahreini R, Froyd KD, Middlebrook AM, McComiskey A, et al. Characteristics, sources, transport of aerosols measured in spring 2008 during the aerosol, radiation, and cloud processes affecting Arctic climate (ARCPAC) project. Atmos Chem Phys 2011;11(6):2423-53.

[18] Wofsy SC. HIAPPER Pole-to-Pole Observations (HIPPO): FIne-grained, global-scale measurements of climatically important atmospheric gases and aerosols. Phil Trans R Soc Lond A 2011;369:2073-86.

[19] Virkkula A, Ahlquist NC, Covert DS, Arnott WP, Sheridan PJ, Quinn PK, et al. Modification, calibration and a field test of an instrument for measuring light absorption by particles. Aerosol Sci Technol 2005;39:68-83.

[20] Schuster GL, Dubovik O, Arola A. Remote sensing of soot carbon - Part 1: Distinguishing different absorbing aerosol species. Atmos Chem Phys 2016;16:1565-85.

[21] Bambha RP, Dansson MA, Schrader PE, Michelsen HA. Effects of volatile coatings and coating removal mechanisms on the morphology of graphitic soot. Carbon 2013;61:80-96.

[22] Charalampopoulos TT, Chang H. Agglomerate parameters and fractal dimension of soot using light scattering: Effects of surface growth. Combust Flame 1991;87:89-99.

[23] Köylü ÜÖ, Faeth GM, Farias TL, Carvalho MG. Fractal and projected structure properties of soot aggregates. Combust Flame 1995;100:621-33.

[24] Oh C, Sorensen CM. The effect of overlap between monomers on the determination of fractal cluster morphology. J Colloid Interface Sci 1997;193:17-25.

[25] Sorensen CM. Light scattering by fractal aggregates: A review. Aerosol Sci Technol 2001;35:648-87.

[26] Kütz S, Schmidt-Ott A. Characterization of agglomerates by condensation-induced restructuring. J Aerosol Sci 1992;23(Suppl. 1):S357-S60.

[27] Miljevic B, Surawski NC, Bostrom T, Ristovski ZD. Restructuring of carbonaceous particles upon exposure to organic and water vapours. J Aerosol Sci 2012;47:48-57.

[28] Saathoff H, Naumann K-H, Schnaiter M, Schöck W, Möhler O, Schurath U, et al. Coating of soot and $(NH_4)_2SO_4$ particles by ozonolysis products of a-pinene. J Aerosol Sci 2003;34:1297-321.

[29] Mikhailov EF, Vlasenko SS, Krämer L, Niessner R. Interaction of soot aerosol particles with water droplets: Influence of surface hydrophility. J Aerosol Sci 2001;32:697-711.

[30] Xue H, Khalizov AF, Wang L, Zheng J, Zhang R. Effects of coating of dicarboxylic acids on the mass-mobility relationship of soot particles. Environ Sci Technol 2009;43:2787-92.

[31] Cross ES, Onasch TB, Ahern A, Wrobel W, Slowik JG, Olfert J, et al. Soot particle studies - Instrument inter-comparison - Project overview. Aerosol Sci Technol 2010;44:592-611.

[32] Spencer MT, Prather KA. Using ATOFMS to determine OC/EC mass fractions in particles. Aerosol Sci Technol 2006;40:585-94.

[33] Lu Z, Hao J, Hu L, Takekawa H. The compaction of soot particles generated by spark discharge in the propene ozonolysis system. J Aerosol Sci 2008;39(10):897-903.

[34] Bueno PA, Havey DK, Mulholland GW, Hodges JT, Gillis KA, Dickerson RR, et al. Photoacoustic measurements of amplification of the absorption cross section for coated soot aerosols. Aerosol Sci Technol 2011;45:1217-30.

[35] Ghazi R, Olfert JS. Coating mass dependence of soot aggregate restructuring due to coatings of oleic acid and dioctyl sebacate. Aerosol Sci Technol 2013;47:192-200.

[36] Slowik JG, Cross ES, Han J-H, Kolucki J, Davidovits P, Williams LR, et al. Measurements of morphology changes of fractal soot particles using coating and denuding experiments: Implications for optical absorption and atmospheric lifetime. Aerosol Sci Technol 2007;41.

[37] Witze PO, Gershenzon M, Michelsen HA. Dual-laser LIDELS: An optical diagnostic for time-resolved volatile fraction measurements of diesel particulate emissions. Proc SAE 2005:SAE Paper no. 2005-01-3791.

[38] Zhang R, Khalizov AF, Pagels J, Zhang D, Xue H, McMurry PH. Variability in morphology, hygroscopicity, and optical properties of soot aerosols during atmospheric processing. Proc Natl Acad Sci U S A 2008;105(30):10291-6.

[39] Khalizov AF, Xue H, Wang L, Zheng J, Zhang R. Enhanced light absorption and scattering by carbon soot aerosol internally mixed with sulfuric acid. J Phys Chem 2009;113:1066-74.

[40] Pagels J, Khalizov AF, McMurry PH, Zhang R. Processing of soot by controlled sulphuric acid and water condensation-Mass and mobility relationship. Aerosol Sci Technol 2009;43:629-40.

[41] Dec JE, zur Loye AO, Siebers DL. Soot distribution in a D. I. diesel engine using 2-D laser-induced incandescence imaging. SAE Trans 1991;100(3):277-88.

[42] Pinson JA, Mitchell DL, Santoro RJ. Quantitative, planar soot measurements in a D. I. diesel engine using laser-induced incandescence and light scattering. Proc SAE 1993:SAE Paper No. 932650.

[43] Fujimoto H, Kurata K, Asai G, Senda J. OH radical generation and soot formation/oxidation in DI diesel engine. Proc SAE 1998:SAE Paper No. 982630.

[44] Inagaki K, Takasu S, Nakakita K. In-cylinder quantitative soot concentration measurement by laser-induced incandescence. SAE Trans 1999;108(3):574-86.

[45] Hertler D, Stirn R, Arndt S, Grzeszik R, Dreizler A. Investigations of soot formation in an optically accessible gasoline direct injection engine by means of laser-induced incandescence (LII). Appl Phys B 2011;104:399-407.

[46] Kock BF, Tribalet B, Schulz C, Roth P. Two-color time-resolved LII applied to soot particle sizing in the cylinder of a diesel engine. Combust Flame 2006;147:79-92.

[47] Zhao H, Ladommatos N. Optical diagnostics for soot and temperature measurement in diesel engines. Prog Energy Combust Sci 1998;24(3):221-55.

[48] Tait NP, Greenhalgh DA. PLIF imaging of fuel fraction in practical devices and LII imaging of soot. Ber Bunsenges Phys Chem 1993;97:1619-25.

[49] Allouis C, D'Alessio A, Noviello C, Beretta F. Time resolved laser induced incandescence for soot and cenospheres measurements in oil flames. Combust Sci Technol 2000;153:51-63.

[50] Axelsson B, Collin R, Bengtsson P-E. Laser-induced incandescence for soot particle size measurements in premixed flat flames. Appl Opt 2000;39:3683-90.

[51] Vander Wal RL, Ticich TM, Stephens AB. Optical and microscopy investigations of soot structure alterations by laser-induced incandescence. Appl Phys B 1998;67:115-23.

[52] Cignoli F, Benecchi S, Zizak G. Time-delayed detection of laser-induced incandescence for the two-dimensional visualization of soot in flames. Appl Opt 1994;33:5778-82.

[53] Shaddix CR, Smyth KC. Quantitative measurements of enhanced soot production in steady and flickering methane/air diffusion flames. Combust Flame 1994;99:723-32.

[54] Snelling D, Thomson KA, Smallwood GJ, Gülder ÖL. Two-dimensional imaging of soot volume fraction in laminar diffusion flames. Appl Opt 1999;38(12):2478-85.

[55] Witze PO, Chase RE, Maricq MM, Podsiadlik DH, Xu N. Real-time measurements of exhaust PM for FTP-75: Comparison of LII, ELPI, and TEOM techniques. Proc SAE 2004:2004-01-0964.

[56] Delhay J, Desgroux P, Therssen E, Bladh H, Bengtsson P-E, Hönen H, et al. Soot volume fraction measurements in aero-engine exhausts using extinction-calibrated backward laser-induced incandescence. Appl Phys B 2009;95:825-38.

[57] Johnson MP, Hilton M, Waterman DR, Black JD. Development of techniques to characterize particulates emitted from gas turbine exhausts. Meas Sci Technol 2003;14:1146-50.

[58] Liggio J, Gordon M, Smallwood GJ, Li S-M, Stroud C, Staebler R, et al. Are emissions of black carbon from gasoline vehicles underestimated? Insights from near and on-road measurements. Environ Sci Technol 2012;46:4819-28.

[59] Sedlacek III AJ, Lewis ER, Kleinman L, Xu J, Zhang Q. Determination of and evidence for non-core-shell structure of particles containing black carbon using the Single-Particle Soot Photometer (SP2). Geophys Res Lett 2012;39:L06802.

[60] Schwarz JP, Gao RS, Fahey DW, Thomson DS, Watts LA, Wilson JC, et al. Single-particle measurements of midlatitude black carbon and light-scattering aerosols from the boundary layer to the lower stratosphere. J Geophys Res 2006;111:D16207.

[61] Subramanian R, Kok GL, Baumgardner DG, Clarke A, Shinozuka Y, Campos TL, et al. Black carbon over Mexico: The effect of atmospheric transport on mixing state, mass absorption cross section, and BC/CO ratios. Atmos Chem Phys 2010;10:219-37.

[62] Canagaratna MR, Jayne JT, Jimenez J-L, Allan JD, Alfarra MR, Zhang O, et al. Chemical and microphysical characterization of ambient aerosols with the Aerodyne aerosol mass spectrometer. Mass Spectrom Rev 2007;26:185-222.

[63] Baumgardner DG, Kok G, Raga G. Warming of the Arctic lower stratosphere by light absorbing particles. Geophys Res Lett 2004;31:L06117.

[64] McMeeking GR, Hamburger T, Liu D, Flynn M, Morgan WT, Northway MJ, et al. Black carbon measurements in the boundary layer over western and northern Europe. Atmos Chem Phys 2010;10:9393-414.

[65] Michelsen HA, Schulz C, Smallwood GJ, Will S. Laser-induced incandescence: Particle diagnostics for combustion, atmospheric, and industrial applications. Prog Energy Combust Sci 2015;51:2-48.

[66] Filippov AV, Zurita M, Rosner DE. Fractal-like aggregates: Relation between morphology and physical properties. J Colloid Interface Sci 2000;229:261-73.

[67] Liu F, Smallwood GJ, Snelling DR. Effects of primary particle diameter and aggregate size distribution on the temperature of soot particles heated by pulsed lasers. J Quant Spectrosc Radiat Transfer 2005;93:301-12.

[68] Liu F, Yang M, Hill FA, Snelling DR, Smallwood GJ. Influence of polydisperse distributions of both primary particle and aggregate size on soot temperature in low-fluence LII. Appl Phys B 2006;83(3):383-95.

[69] Kuhlmann S-A, Reimann J, Will S. On the heat conduction between laser-heated nanoparticles and a surrounding gas. J Aerosol Sci 2006;37:1696-716.

[70] Bladh H, Johnsson J, Bengtsson P-E. On the dependence of the laser-induced incandescence (LII) signal on soot volume fraction for variations in particle size. Appl Phys B 2008;90:109-25.

[71] Bladh H, Johnsson J, Rissler J, Abdulhamid H, Olofsson N-E, Sanati M, et al. Influence of soot particle aggregation on time-resolved laser-induced incandescence signals. Appl Phys B 2011;104:331-41.

[72] Johnsson J, Bladh H, Olofsson N-E, Bengtsson P-E. Influence of soot aggregate structure on particle sizing using laser-induced incandescence: Importance of bridging between primary particles. Appl Phys B 2013;112(3):321-32.

[73] Daun KJ. Effect of selective accommodation on soot aggregate shielding in time-resolved laser-induced incandescence experiments. J Heat Transfer 2010;132:091202.

[74] Snelling DR, Liu F, Smallwood GJ, Gülder ÖL. Determination of the soot absorption function and thermal accommodation coefficient using low-fluence LII in a laminar coflow ethylene diffusion flame. Combust Flame 2004;136:180-90.

[75] Bambha RP, Dansson MA, Schrader PE, Michelsen HA. Effects of volatile coatings on the laser-induced incandescence of soot. Appl Phys B 2013;112(3):343-58.

[76] Liou KN, Takano Y, Yang P. Light absorption and scattering by aggregates: Application to black carbon and snow grains. J Quant Spectrosc Radiat Transfer 2011;112:1581-94.

[77] Colbeck I, Appleby L, Hardman EJ, Harrison RM. The optical properties and morphology of cloud-processed carbonaceous smoke. J Aerosol Sci 1990;21(4):527-38.

[78] Liu L, Mishchenko MI, Arnott WP. A study of radiative properties of fractal soot aggregates using the superposition T-matrix method. J Quant Spectrosc Radiat Transfer 2008;109:2656-63.

[79] Frey J, Pinvidic JJ, Botet R, Jullien R. Light scattering by fractal aggregates: A numerical investigation. Journal de Physique France 1988;49:1969-76.

[80] Michelsen HA. Understanding and predicting the temporal response of laser-induced incandescence from carbonaceous particles. J Chem Phys 2003;118(15):7012-45.

[81] Michelsen HA, Liu F, Kock BF, Bladh H, Boiarciuc A, Charwath M, et al. Modeling laser-induced incandescence of soot: A summary and comparison of LII models. Appl Phys B 2007;87:503-21.

[82] López-Yglesias X, Schrader PE, Michelsen HA. Soot maturity and absorption cross sections. J Aerosol Sci 2014;75:43-64.

[83] Bambha RP, Michelsen HA. Effects of aggregate morphology on size and laser-induced incandescence and scattering from black carbon (mature soot). J Aerosol Sci 2015;88:159-81.

[84] Moteki N, Kondo Y. Method to measure time-dependent scattering cross sections of particles evaporating in a laser beam. J Aerosol Sci 2008;39:348-64.

[Blank page following section.]

DISTRIBUTION

1	MS0701	Peter Davies	6900
1	MS0734	Dan Lucero	6913
1	MS0734	Mark Ivey	6913
1	MS0750	Amy Halloran	6913
1	MS9033	David Reyna	8128
1	MS9053	Ray Bambha	8128
1	MS9054	Bob Hwang	8300
1	MS9054	Sarah Allendorf	8350
1	MS9055	Craig Taatjes	8353
1	MS9055	Hope Michelsen	8353
1	MS9055	Paul Schrader	8353

1	MS0899	Technical Library	9536 (electronic copy)

For LDRD reports, add:

1	MS0359	D. Chavez, LDRD Office	1911

For CRADA reports add:

1	MS0115	OFA/NFE Agreements	10012

For Patent Caution reports, add:

1	MS0161	Legal Technology Transfer Center	11500


Sandia National Laboratories